

On the vortex motion in high temperature superconductors

I. L. Landau and H. R. Ott

Laboratorium für Festkörperphysik, ETH Hönggerberg, CH-8093 Zürich, Switzerland

(October 27, 2018)

We show that prominent features in voltage-current characteristics, recently measured in the mixed state of high- T_c superconductors and interpreted as evidence for an irreversibility line or a vortex-glass transition, may very well be explained with the simplest Kim-Anderson approach describing the vortex motion. In this case, the irreversibility line is not related to a transition in the system of vortices. Consulting numerous experimental reports on this subject we have not found a single example, which is in contradiction with this view.

PACS numbers: 74.60.Ge, 74.60.Jg, 74.72.-h

I. INTRODUCTION

The commonly accepted picture of the magnetic flux motion in high temperature superconductors (HTSC) is extremely complex. Many different theoretical models have been developed in order to explain various aspects of the flux-creep process (see Ref. 1 for details). The complexity of the models that have been invented to capture the motion of vortices in HTSC is related to the apparent inability of the simple Kim-Anderson approach for explaining the experimental results.^{2,3} However, a serious reconsideration of available data indicates that this may not really be the case. Recent experiments have shown that the low-temperature flux-creep data may perfectly well be described using the Kim-Anderson approach, if a realistic profile of the pinning potential is taken into account.⁴⁻⁶ In this paper we use a similar approach to analyze the motion of vortices at temperatures close to the superconducting critical temperature T_c . We show that the very specific features in voltage-current characteristics that manifest the flux-creep process and which are usually related to the irreversibility line and a vortex-glass transition, not only may be explained by employing the Kim-Anderson approach, but are a direct consequence of this simple model. First, we briefly recapitulate the model and its consequences and subsequently address some issues concerning the irreversibility line and the vortex-glass transition.

II. THE MODEL

If the current density j in a sample is less than its critical value j_c , all vortices are pinned and their motion is only due to a thermally activated hopping of the vortex lines over potential barriers or via quantum tunneling through the barriers. The probability of hopping in the case of thermal activation is

$$w = \nu_0 \exp\left(-\frac{U}{k_B T}\right), \quad (1)$$

where ν_0 is the attempt frequency of the vortex line to surmount the potential barrier of height U and k_B is the

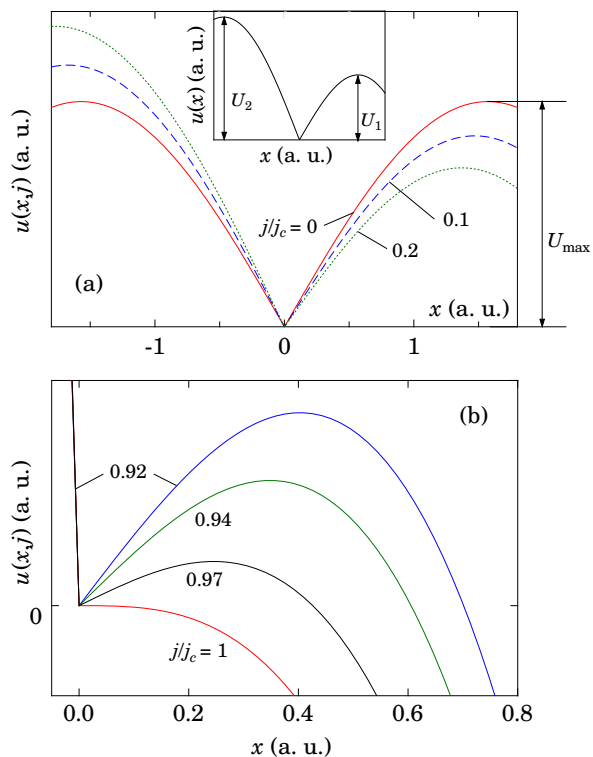


FIG. 1. Schematic profiles of a pinning well for different values of the current density. The corresponding values of j/j_c are indicated near the curves. (a) $j/j_c \ll 1$. Inset illustrates definitions of U_1 and U_2 . (b) $1 - j/j_c \ll 1$.

Boltzmann constant.

As an example, a pinning-potential profile proportional to $|\sin x|$ is shown by the solid line in Fig. 1(a). At a given temperature T , the profile of the potential well for $j = 0$ may be written as

$$u(x) = U(T)f(x, T), \quad (2)$$

where $U(T)$ is the energy fixing the pinning strength and the function $f(x, T)$ defines the shape of the potential well, which may be temperature dependent as well. We

have chosen f such that $|df/dx|$ is maximum at $x = 0$, the site of the minimum of a single well. $U(T)$ decreases with increasing temperature and it vanishes at the temperature at which the external magnetic field H is equal to the upper critical field H_{c2} . In the following, U_{\max} denotes the maximum value of $u(x, j = 0)$ between two local minima as is illustrated in Fig. 1(a). Also U_{\max} is decreasing with increasing T but its temperature dependence may differ from that of $U(T)$.

An electric current does not change the interaction of a vortex with the pinning centers or other vortices, but it causes a Lorentz force F_L to act on the vortices. The Lorentz force tilts the potential profile, thus reducing the potential barriers in the direction of the vortex motion. In the presence of a current the potential profile may be written as

$$u(x, j) = u(x, 0) - xF_L \quad (3)$$

with $F_L = j\Phi_0/c$, j as the current density, Φ_0 the magnetic flux quantum, and c the speed of light. The critical current density is reached if the potential barriers vanish. According to Eqs. (2) and (3), this results in

$$j_c(T) = \frac{cU(T)f'_c}{\Phi_0}, \quad (4)$$

where f'_c is the maximum value of $|df/dx|$. As stated above, $|df/dx|$ reaches its maximum at $x = 0$, i.e., $f'_c = |df/dx|_{x=0}$. Equation (4) is a formal definition of the critical current density, the only appropriate definition of j_c that may be given in the mixed state of type-II superconductors. As will be shown in section IV (see Fig. 6a), at temperatures close to the superconducting critical temperature T_c , the sample resistance in the mixed state may be rather high even if $j \ll j_c$. This is the reason why different voltage criteria for the evaluation of the critical current density, although useful for practical purposes, are rather meaningless from the point of view of physics.

The influence of current on the potential profile is illustrated in Figs. 1(a) and 1(b). It may be seen that at low currents ($j \ll j_c$) the decrease of the activation energy with increasing current is entirely determined by the behavior of $u(x)$ near its maximum [see Fig. 1(a)], while at currents close to j_c only $u(x)$ in the vicinity of $x = 0$ is important [see Fig. 1(b)]. We denote the heights of potential barriers in the direction of the Lorentz force and opposite to it by U_1 and U_2 , respectively [see inset to Fig. 1(a)]. For a non-zero current, $U_1 < U_2$. The electrical field E in the sample is proportional to the average velocity of vortices and may be written as

$$E = E_0 \left[\exp\left(-\frac{U_1(T, j)}{k_B T}\right) - \exp\left(-\frac{U_2(T, j)}{k_B T}\right) \right] \quad (5)$$

with

$$E_0 = \frac{B}{c} l v_0. \quad (6)$$

Here B is the magnetic induction in the sample and l is the vortex hopping distance. The second term in Eq. (5) describes the vortex hopping in the direction opposite to the Lorentz force. This term is only important for $j/j_c \ll 1$ and at high temperatures.⁷

If the function f in Eq. (2) is known, U_1 and U_2 may be deduced by using Eq. (3). In practice however, the situation is quite different. The main goal is rather to obtain information about $u(x)$ from experimental results. In most cases, the experimentally accessible information is limited to $E(j)$ curves, measured at different temperatures. In order to obtain any useful information about $u(x)$ from these experimental data, some *a priori* assumptions have to be made. As has been shown recently, the flux-creep rates in an epitaxial $\text{YBa}_2\text{Cu}_3\text{O}_{7-x}$ (YBCO) film may be very well described in a wide range of temperatures ($0.02T_c \leq T \leq 0.9T_c$) with the assumption that not the shape, but only the amplitude of the $u(x)$ function is temperature dependent.⁴⁻⁶ In this case, the function f in Eq. (2) depends only on x and the temperature dependencies of U_{\max} and $U(T)$ coincide. Based on this assumption, a scaling procedure for the analysis of flux-creep data has been established.⁴⁻⁶ It is an important advantage of this approach that it allows for internal consistency checks and all assumptions that have been made may be verified retrospectively. It turns out that the scaling procedure breaks down at $T \geq 80\text{K} \approx 0.9T_c$.⁶ This demonstrates that the assumption of a temperature independent f function is not valid close to the critical temperature and therefore should be abandoned in this temperature range.

In the following we use Eq. (5) to analyze the voltage-current characteristics of the sample at temperatures close to T_c . It will be shown that different consequences of the vortex motion, such as the vanishing of the persistent current at $T_{irr} < T_c$ (irreversibility line) and the often observed sign change in the curvature of the $\log E - \log j$ curves with increasing temperature, which is usually attributed to a vortex-glass transition, follow straightforwardly from Eq. (5) without any additional assumption.

III. IRREVERSIBILITY LINE

Among numerous unusual features of HTSC, the so-called irreversibility line (IRL) has attracted a lot of attention. This line in the $H - T$ phase diagram separates two regions with distinctly different behavior.⁸⁻¹⁵ Above the IRL the magnetization of the sample is reversible, which means that the sample cannot carry any persistent current. Below the IRL, irreversible magnetization is observed. Since the true superconducting state with zero dissipation is achieved only below the IRL, the position of this line in the $H - T$ diagram is extremely important for applications. However, in spite of many years of intensive studies, the situation with regard to the IRL

is far from being clear. Not only the origin of the IRL is still under discussion, but there is also no consensus concerning valid procedures to establish the position of the IRL from the experimental data.

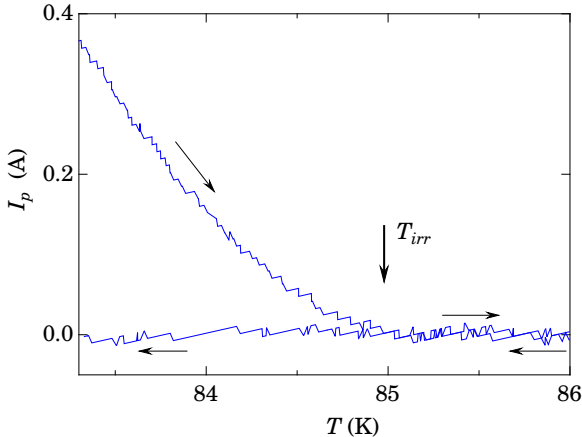


FIG. 2. Persistent current I_p in a ring-shaped $\text{YBa}_2\text{Cu}_3\text{O}_{7-x}$ film as a function of temperature (description of the sample may be found in Ref. 4). The vertical arrow indicates the position of the irreversibility temperature as given by the present experiment. The sample was cooled in an external magnetic field $H \approx 1000$ Oe to $T = 82$ K. The current was subsequently induced by enhancing the magnetic field by 1 Oe.

In order to make the physics more transparent, we consider here a ring-shaped sample. In this case the persistent current in the sample I_p plays the role of an irreversible magnetic moment M_{irr} . The current in the ring may easily be monitored by measuring the magnetic induction in the ring cavity using, for instance, a Hall probe placed in the center of the cavity. Typical experimental data for a ring-shaped sample obtained from an epitaxial YBCO film are presented in Fig. 2. This figure shows a heating-cooling cycle of I_p . Our data in Fig. 2, as well as results of measurements of the irreversible magnetization,^{8–15} reveal that above the irreversibility temperature, T_{irr} , the persistent current is essentially zero. This is why T_{irr} is usually considered as the temperature, at which the critical current density vanishes. It is commonly accepted that T_{irr} corresponds to some transition invoking the vortex system of the sample. Among a few considered possibilities for such a transition, the melting of a vortex-glass phase is the most popular explanation for the irreversibility line in HTSC.¹⁸ However, as shown below, this kind of temperature dependence of the persistent current I_p necessarily follows from the simplest Kim-Anderson approach for describing the flux-creep process.

At temperatures well below the IRL the situation is quite clear. All vortices are pinned and their motion only occurs due to a thermally activated hopping of vor-

tex lines over potential barriers. According to Eq. (1) the probability of hopping depends exponentially on $U/k_B T$. Equation (1) implies that the resistance of a type-II superconductor in the mixed state formally never vanishes. However, at low temperatures and small currents, the ratio $U/k_B T$ is so large that the probability of hopping is negligible. In this case, an electric current induced in a ring-shaped sample may flow without a noticeable decay for years. Because the ratio $U/k_B T$ decreases rapidly when approaching T_c , the current-decay rate increases significantly with increasing temperature.

The current decay rate dj/dt is proportional to the electrical field in the sample and therefore Eq. (5) may be used for evaluating this important quantity. In order to calculate the temperature and current dependencies of dj/dt , we have to assume some explicit expression for the profile of the potential well $u(x)$. Unfortunately, practically nothing is known about $u(x)$ in this high temperature range. In our previous study it was shown that the function f in Eq. (2) may be considered as temperature independent only for $T < 0.9T_c$.⁶ For higher temperatures the temperature dependence of f has to be taken into account. In the following analysis we have chosen two rather different representations for $f(x, T)$, i.e.,

$$f(x, T) = |x| - a(1 - T/T_c)^k x^2 \quad (7)$$

and

$$f(x, T) = \left(\sqrt{|x| + x_0} - \sqrt{x_0} \right) - b \frac{(|x| + x_0)^{3/2} - x_0^{3/2}}{(1 - T/T_c)^m}, \quad (8)$$

with

$$U(T) = U_0(1 - T/T_c)^{3/2} \quad (9)$$

for both cases. This kind of $U(T)$ follows from the simplest consideration of the vortex pinning at temperatures close to T_c .^{16,17} The potential profiles represented by Eqs. (7) and (8) are depicted in the insets to Fig. 3. We do not pretend that any of the f functions given by Eq. (7) or (8) exactly represent the real situation in HTSC. Our choice of f has been made in view of obtaining a reasonable profile shape and the possibility to perform analytical calculations. As will be shown below, the particular choice of f does not influence the main qualitative features of the flux-creep process.

We may now insert the potential profiles given by Eqs. (7) to (9) into Eq. (2) and calculate $U_1(T, j)$ and $U_2(T, j)$ with the help of Eq. (3). Substituting the resulting expressions for U_1 and U_2 into Eq. (5), we obtain the corresponding temperature and current dependencies of the electrical field E in the sample. In order to compare the results of this calculation with the experimental data presented in Fig. 2, we need an evaluation of E_0 and U_0 entering Eqs. (5) and (9), respectively. For this purpose, we calibrated our calculated $E(j)$ via a voltage-current characteristic measured for the same sample at

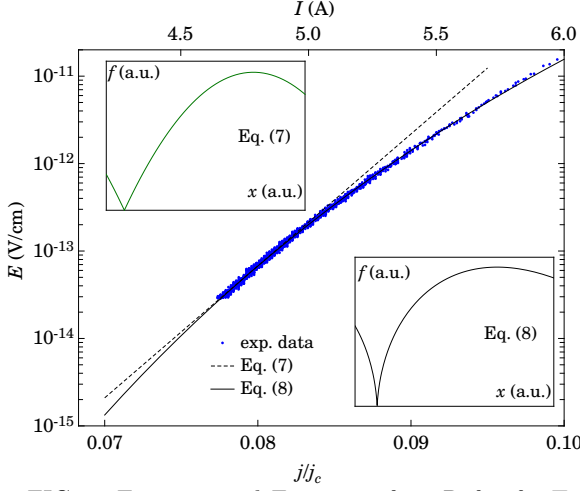


FIG. 3. Experimental $E-j$ curve from Ref. 6 for $T = 0.9T_c$ and $H = 0.9$ kOe. The lines are approximations to this curve using Eqs. (7) and (8) for the profile of the potential well. The upper scale shows absolute values of the current. The upper and lower insets show examples of the profiles of the potential well as given by Eqs. (7) and (8), respectively.

$T = T_0 \approx 0.9T_c$.⁶ Fig. 3 shows the experimental data together with the calculated $E(j)$ curves using $f(x, T)$ as given by Eqs. (7) and (8), respectively. In the first case, the constants E_0 in and U_0 were adjusted such as to approximate the low voltage part of the $E(j)$ curve; the constant $a = (1 - T_0/T_c)^{-k}$. In the second case, the parameters x_0 and b in Eq. (8) were used as fitting

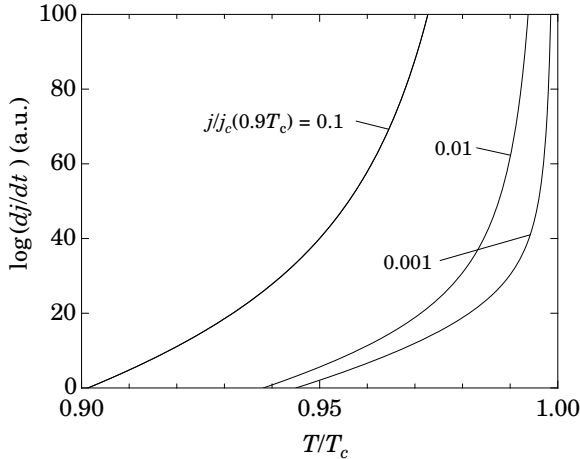


FIG. 4. Calculated variation of dj/dt versus T/T_c for $f(x, T)$ given by Eq. (7) with $k = 1.4$. Calculations were made for 3 fixed current densities. The values of the renormalized current densities $j/j_c(0.9T_c)$ are indicated near the curves.

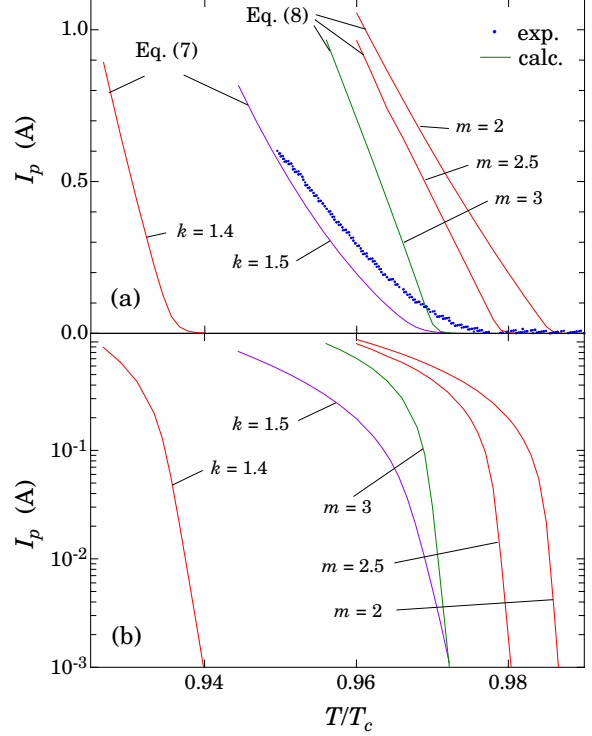


FIG. 5. I_p as a function of temperature. The solid lines are results of calculations for different representations of $u(x)$. (a) On linear scales, the points represent the experimental data from Fig. 2. (b) $\log I_p$ versus T/T_c .

parameters, as well.

Using these adjusted expressions for E , we may now calculate different characteristics of the sample for the chosen $f(x, T)$. Fig. 4 shows the temperature dependencies of $dj/dt \propto E$ for three values of the current density. In this particular case, the calculation was made for $f(x, T)$ given by Eq. (7) with $k = 1.4$. Note that we use a log-scale for the dj/dt -axis and that the total change in dj/dt is 100 orders of magnitude. This figure clearly demonstrates that dj/dt grows extremely fast with increasing temperature close to T_c . This implies that a current which is practically constant in time at a certain temperature, will be decaying rather quickly at a slightly enhanced temperature.

Experimentally the persistent current I_p is usually determined as the current which is not decaying during the time of the experiment. This definition of the persistent current is not universal because the value of I_p is obviously dependent on the experimental resolution and the time window of the particular experiment. In our approach we can calculate the temperature dependence of the persistent current by choosing dI/dt as set by the available resolution of the experiment. The following calculations were made for $dI/dt = 3 \cdot 10^{-4}$ A/s, which is the resolution for the experimental data presented in Fig.

2. In order to demonstrate how the $I_p(T) \propto M_{irr}(T)$ curve depends on the particular choice of the potential profile, the calculations were made for both approximations of $f(x, T)$ and for different values of the exponents k and m in Eqs. (7) and (8), respectively. The results of the calculations, together with experimental data from Fig. 2, are shown in Figs. 5(a) and 5(b). It may be seen that, depending on the degree of experimental resolution, an "irreversibility" temperature exists for all the chosen functions $f(x, T)$. At the same time, both the shape of the $I_p(T)$ curves and the position of T_{irr} are rather sensitive to the choice of f . This means that by a proper choice of $U(T)$ and $f(x, T)$ in Eq. (2), any experimentally observed temperature dependence of the irreversible magnetic moment $M_{irr}(T)$ or the persistent current $I_p(T)$ may be approximated to a high degree of accuracy and no specific transition in the vortex system is needed to explain the existence of the irreversibility line established in this way.

IV. VORTEX-GLASS TRANSITION

As has been mentioned above, the most popular interpretation of the irreversibility line in the $H - T$ diagram is that it is a manifestation of a vortex-glass transition.^{8,18,19} Many experimental results seem to confirm the concept of a vortex-glass melting at temperatures close to the IRL.^{12,20-29} In this section we show that the distinct variation of the shape of the $\log E - \log j$ curves, which is usually interpreted as a manifestation of the vortex-glass melting, follows straightforwardly from our simple consideration outlined in the previous section.

To make the point, we use $f(x, T)$ as given by Eq. (8) with $m = 2$. The results of the calculations of $E(j)$ are shown in Fig. 6(a) as $E(j)$ curves at fixed temperatures. Qualitatively this plot is indistinguishable from numerous experimental results (see Refs. 20-29) and it is clear that by corresponding adjustments of $U(T)$ and $f(x, T)$, any experimental $E(j, T)$ curve may be approximated even quantitatively by this type of calculation. Fig. 6(b) shows the same $E(j)$ curves as Fig. 6(a) at much lower voltages. It may be seen that the change of the curvature, which is usually attributed to the vortex-glass transition, is a universal feature of the $E(j)$ curves at temperatures close to T_c . With decreasing temperature however, the sign change of the curvature is shifted to lower voltages where it is not accessible experimentally.

We emphasize that the crossover to ohmic $E(j)$ curves with decreasing current is independent of the particular choice of the $u(x)$ function. As has been demonstrated in Section II, for $j/j_c \ll 1$, only a small part of the $u(x)$ function near its maximum is important. In this region, $u(x, 0)$ may be replaced by a Taylor expansion of the form

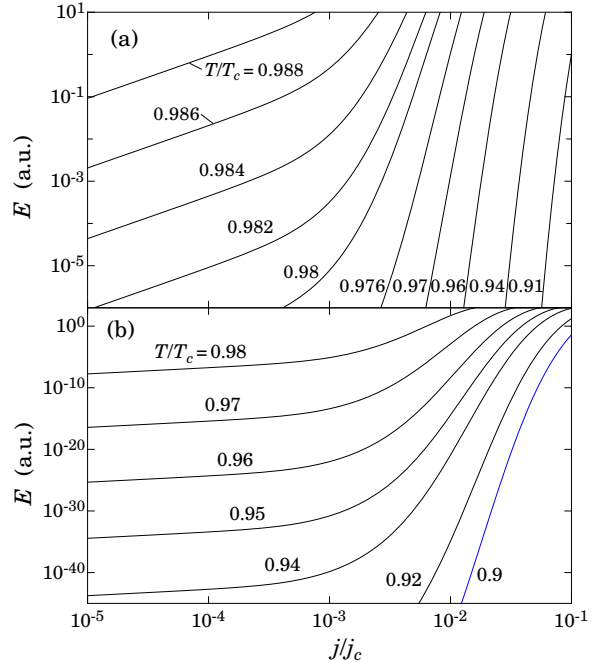


FIG. 6. (a) and (b) $E - j$ curves calculated for $f(x, T)$ given by Eq. (8) with $m = 2$ and parameters x_0 and b determined as is explained in the previous section.

$$u(x) = U_{\max} \left[1 - \frac{A^2}{2} \left(\frac{|x|}{x_0} - 1 \right)^2 \right]. \quad (10)$$

Here x_0 is the point where $u(x, 0)$ has its maximum and A is the curvature of u at $x = x_0$. Both A and x_0 may be temperature dependent. Using Eqs. (3) and (10), the activation energies are

$$U_{1,2} = U_{\max} \left[1 \mp j \frac{x_0 \Phi_0}{cU_{\max}} + \frac{j^2}{2} \left(\frac{x_0 \Phi_0}{cAU_{\max}} \right)^2 \right]. \quad (11)$$

Inserting (11) into Eq. (5), we get

$$E = E_0 \exp \left(-\frac{U_{\max}}{k_B T} \right) \exp \left[\frac{(jx_0 \Phi_0 / cA)^2}{2k_B T U_{\max}} \right] \sinh \left(\frac{jx_0 \Phi_0}{ck_B T} \right). \quad (12)$$

Because of the additional exponential term, the j dependence of E cannot be reduced to a hyperbolic sinus.⁷ Taking into account that Eq. (12) is only valid at the low-current limit, we may use the expansions of the exponential and hyperbolic sinus functions and neglect all terms j^n ($n \geq 2$). Eq. (12) is thus reduced to

$$E = j \frac{x_0 \Phi_0}{ck_B T} E_0 \exp \left(-\frac{U_{\max}}{k_B T} \right) \quad (13)$$

and hence at any temperature, the sample resistivity $\rho = E/j$ is independent of the current density for $j \ll j_0 = cU_{\max}/x_0 \Phi_0$.

A very similar explanation of the voltage-current characteristics near the "vortex-glass" transition has been suggested by Coppersmith et al.³⁰ In their short comment they considered a sinusoidal potential barrier. It was shown that even with this simple potential all the qualitative features of the experimental $E(j)$ curves could be reproduced. The authors also pointed out that the insignificant quantitative disagreement with the experimental data is simply due to the arbitrary chosen sinusoidal profile of the potential barriers.

V. CONCLUSION

As has been shown in Sections III and IV, the experimentally established vanishing of the persistent current at $T = T_{irr} < T_c(H)$ does not necessarily mean that the critical current density vanishes at $T \geq T_{irr}$ and no singular event, such as a vortex-glass transition, needs to be involved in order to explain the experimentally verifiable disappearance of the irreversible magnetization at the irreversibility line. This feature, as well as the change of curvature of the voltage-current characteristics with temperature, which is usually considered as a manifestation of the vortex-glass melting, automatically follow from the simplest consideration of thermally activated vortex motion (see Figs. 5 and 6).

In experimental papers dealing with vortex-glass melting, there is usually no discussion of alternative possibilities to account for the experimental results. All the data are scaled according to the vortex-glass model and the corresponding correlation lengths are determined. A common statement in most of these papers is that the flux-creep model cannot provide a negative curvature for the low temperature $\log E - \log j$ curves.^{22,23} As may be seen in Figs. 6(a) and 6(b), a negative curvature may very well be accounted for by the flux creep model. In a treatment of thermally activated vortex hopping given in Section IV, this curvature depends on the particular pinning potential.

The latter expression is based on a linear dependence of the activation energy on j and is widely used in the literature.^{1,31} However, it is valid for triangular potential barriers only (see Refs. 4 and 6 for details).

-
- ¹ G. Blatter, M. V. Feigel'man, V. B. Geshkenbein, A. I. Larkin, and V. M. Vinokur, *Rev. Mod. Phys.*, **42**, 1125 (1994).
² Y. B. Kim, C. F. Hempstead, and A. R. Strand, *Phys. Rev. Lett.* **9**, 306 (1962).
³ P. W. Anderson, *Phys. Rev. Lett.* **9**, 309 (1962).
⁴ I. L. Landau and H. R. Ott, *Physica C* **331**, 1 (2000).
⁵ I. L. Landau and H. R. Ott, *Physica C* **340**, 251 (2000).
⁶ I. L. Landau and H. R. Ott, *Phys. Rev. B* **63**, 184516 (2001).
⁷ For any smooth potential profile $u(x)$, Eq. (5) cannot be reduced to $E = E_0 \exp(-U/k_B T) \sinh([(U/k_B T)(j/j_c)])$.

- ⁸ K. A. Müller, M. Takashige, and J. G. Bednorz, *Phys. Rev. Lett.* **58**, 1143 (1987).
⁹ A. Schilling, H. R. Ott, and Th. Wolf, *Phys. Rev. B* **46**, 14253 (1992).
¹⁰ Hai-hu Wen and Zhong-xian Zhao, *Phys. Rev. B* **50**, 13853 (1994).
¹¹ A. Neminsky, J. Dumas, B. P. Thrane, C. Schlenker, H. Karl, and B. Stritzker, *Phys. Rev. B* **50**, 3307 (1994).
¹² J. Deak, M. McElfresh, J. R. Clem, Z. Hao, M. Konczykowski, R. Muenchausen, S. Foltyn, and R. Dye, *Phys. Rev. B* **49**, 6270 (1994).
¹³ M. C. Frischherz, F. M. Sauerzopf, H. W. Weber, M. Murakami, and, G. A. Emelchenko, *Supercon. Sci. Technol.* **8**, 485 (1995).
¹⁴ Terukazu Nishizaki, Tomoyuki Naito, and Norio Kobayashi, *Phys. Rev. B* **58**, 11169 (1998). Terukazu Nishizaki and Norio Kobayashi, *Supercond. Sci. Technol.* **13**, 1 (2000).
¹⁵ H. H. Wen, S. L. Li, and Z. X. Zhao, *Phys. Rev. B* **62**, 716 (2000).
¹⁶ Y. Yeshurun and A. P. Malozemoff, *Phys. Rev. Lett.* **60**, 2202 (1988).
¹⁷ M. Tinkham, *Phys. Rev. Lett.* **61**, 1658 (1988).
¹⁸ M. P. A. Fisher, *Phys. Rev. Lett.* **62**, 1415 (1989).
¹⁹ D. S. Fisher, M. P. A. Fisher, D. A. Huse, *Phys. Rev. B* **43**, 130 (1991).
²⁰ R. H. Koch, V. Foglietti, W. J. Gallagher, G. Koren, A. Gupta, and M. P. A. Fisher, *Phys. Rev. Lett.* **63**, 1511 (1989).
²¹ J. Deak, M. McElfresh, John R. Clem, Zhidong Hao, M. Konczykowski, R. Muenchausen, S. Foltyn, and R. Dye, *Phys. Rev. B* **47**, 8377 (1993).
²² H. Yamasaki, K. Endo, S. Kosaka, M. Umeda, S. Yoshida, and K. Kajimura, *Phys. Rev. B* **50**, 12959 (1994).
²³ O. B. Hyun, T. Nabatame, S. Koike, H. Suhara, and I. Hirabayashi, *Phys. Rev. B* **52**, 15545 (1995).
²⁴ M. Friesen, J. Deak, Lifang Hou, and M. McElfresh, *Phys. Rev. B* **54**, 3525 (1996).
²⁵ Hai-hu Wen, H. A. Radovan, F.-M. Kamm, P. Ziemann, S. L. Yan, L. Fang, and M. S. Si, *Phys. Rev. Lett.* **80**, 3859 (1998).
²⁶ Akihito Sawa, Hirofumi Yamasaki, Yasunori Mawatari, Haruhiko Obara, Masaichi Umeda, and Shin Kosaka, *Phys. Rev. B* **58**, 2868 (1998).
²⁷ P. Voss-deHaan, G. Jakob, and H. Adrian, *Phys. Rev. B* **60**, 12443 (1999).
²⁸ Z. H. Wang, H. Zhang, and X. W. Cao, *Physica C* **337**, 62 (2000).
²⁹ Y. Z. Zhang, R. Deltour, J. F. de Marneffe, H. H. Wen, Y. L. Qin, C. Dong, L. Li, and Z. X. Zhao, *Phys. Rev. B* **62**, 11373 (2000).
³⁰ S. N. Coppersmith, M. Inui, and P. B. Littlewood, *Phys. Rev. Lett.* **64**, 2585 (1990).
³¹ Ju-Jin Kim, Ho-kyun Lee, Jinwook Chung, Hyun Joon Shin, Hu Jong Lee, and Ja Kang Ku, *Phys. Rev. B* **43**, 2962 (1991).